Journal of Power Sources 195 (2010) 5520–5526

Contents lists available at ScienceDirect

Journal of Power Sources

journal homepage: www.elsevier.com/locate/jpowsour

Synthesis and electrocatalysis of 1-aminopyrene-functionalized carbon nanofiber-supported platinum–ruthenium nanoparticles

Zhan Lin, Liwen Ji, Wendy E. Krause, Xiangwu Zhang*

Fiber and Polymer Science Program, Department of Textile Engineering, Chemistry and Science, North Carolina State University, Raleigh, NC 27695-8301, USA

ARTICLE INFO

Article history:
Received 15 March 2010
Accepted 16 March 2010
Available online 27 March 2010

Keywords:
Electrospinning
Carbon nanofibers
1-Aminopyrene
PtRu nanoparticles
Methanol

ABSTRACT

Platinum–ruthenium/carbon composite nanofibers were prepared by depositing PtRu nanoparticles directly onto electrospun carbon nanofibers using a polyol processing technique. The morphology and size of PtRu nanoparticles were controlled by 1-aminopyrene functionalization. The noncovalent functionalization of carbon nanofibers by 1-aminopyrene is simple and can be carried out at ambient temperature without damaging the integrity and electronic structure of carbon nanofibers. The resulting PtRu/carbon composite nanofibers were characterized by cyclic voltammogram in 0.5 M H_2SO_4 and 0.125 M CH_3OH + 0.2 M H_2SO_4 solutions, respectively. The PtRu/carbon composite nanofibers with 1-aminopyrene functionalization have smaller nanoparticles and a more uniform distribution, compared with those pretreated with conventional acids. Moreover, PtRu/1-aminopyrene functionalized carbon nanofibers have high active surface area and improved performance towards the electrocatalytic oxidation of methanol.

1. Introduction

To meet the ever-increasing energy demands and to tackle the daunting problem of environmental pollution, direct methanol fuel cells (DMFCs) have recently attracted much attention, since they can provide green power for electric vehicles and electronic portable devices by direct conversion of methanol fuel [1–3]. The methanol conversion is carried out in the membrane electrode assembly (MEA, a key component of DMFCs), which consists of a polymer electrolyte membrane and two catalyst-loaded porous electrodes for methanol oxidation at the anode and oxygen reduction at the cathode. The methanol oxidation reaction (MOR) typically is catalyzed by Pt in acidic environment in Eq. (1) [4].

$$CH_3OH + H_2O \rightarrow CO_2 + 6H^+ + 6e^-,$$
$$E^0(\mathrm{MOR}) = 0.016\,\mathrm{V\ vs.\ SHE\ at\ 25\,^\circ C} \quad (1)$$

During this reaction, one of the intermediates, CO, often poisons the Pt catalyst by adsorbing strongly on the surface of the catalyst. In order to remove the adsorbed CO, a high potential is required to oxidize CO by reacting with hydroxide (–OH) produced during water activation, thereby limiting the use of a pure Pt catalyst in DMFCs. Therefore, to provide –OH at lower potentials for the oxidative removal of adsorbed CO, a second metal, *i.e.*, Ru, has been used to form an alloy with Pt to promote the oxidation of CO to CO_2 by a bi-functional mechanism [5,6].

Until now, a major challenge for the commercial application of DMFCs is the high cost of Pt or Pt alloy electrocatalysts [7–12]. Therefore, the development of highly active electrode catalysts coupled with a suitable electrode structure and low catalyst loading is important for attaining high efficiency in DMFCs, and subsequently lowering their cost. Carbon nanomaterials are currently being considered as suitable supports for catalysts in DMFCs [13–15], because of their unique graphite properties combined with three-dimensional flexible structures. Carbon nanofibers (CNFs), one of the promising carbon nanomaterials for supporting catalysts, have been investigated by several research groups due to their unique 1-dimensional structure, high electronic and thermal conductivities, and good electrochemical stability [16,17]. However, since CNFs are chemically inert, the activation of their graphitic surface is necessary because the deposition, distribution, and size of Pt or Pt alloy nanoparticles strongly depend on the surface properties of CNFs [18].

In order to anchor and deposit catalyst nanoparticles on the surface of carbon nanomaterials, many harsh oxidative methods, such as refluxing in concentrated mixtures of H_2SO_4 and HNO_3, and cycling in H_2SO_4 solution using cyclic voltammogram, have been widely utilized. However, these methods result in defects on the carbon nanomaterials, which are harmful to the electrochemical active surface area of Pt or Pt alloy electrocatalysts and their dura-

* Corresponding author at: Fiber and Polymer Science Program, Department of Textile Engineering, Chemistry and Science, North Carolina State University, 2401 Research Drive, Raleigh, NC 27695-8301, USA. Tel.: +1 919 515 6547; fax: +1 919 515 6532.
E-mail address: xiangwu_zhang@ncsu.edu (X. Zhang).

0378-7753/$ – see front matter © 2010 Elsevier B.V. All rights reserved.
doi:10.1016/j.jpowsour.2010.03.059

bility during fuel cell operation [19]. Recently, novel noncovalent functionalization methods of carbon nanomaterials, such as coating carbon nanotubes (CNTs) with 1% sodium dodecyl sulfate [20] or functionalizing CNTs with 1-aminopyrene [21], have attracted particular attention because they enable the surface activation of carbon nanomaterials without destroying their intrinsic properties [22–24]. However, until now no studies on the functionalization of CNFs using such noncovalent methods have been reported.

In this paper, we prepared and characterized PtRu/carbon composite nanofibers (PtRu/CNFs) by the combination of 1-aminopyrene functionalization and a polyol processing technique. We functionalized electrospun carbon nanofibers with 1-aminopyrene, followed by the deposition of PtRu using ethylene glycol as a reducing agent. The most important advantage of this approach is that the 1-aminopyrene functionalization treatment preserves the integrity and the electronic structure of CNFs, which result in the long-term stability of such composites in the application of DMFCs. Moreover, PtRu nanoparticles with small diameter and homogenous distribution are obtained, and high electrochemical surface area and good activity toward methanol oxidation also are observed on the resultant PtRu/CNFs.

2. Experimental

2.1. Chemicals and reagents

Polyacrylonitrile (PAN), N,N-dimethylformamide (DMF), chloroplatinic acid hydrate ($H_2PtCl_6{\cdot}xH_2O$), ruthenium chloride ($RuCl_3$), 1-aminopyrene (1-AP), ethylene glycol (EG), nitric acid (HNO_3, 70%), sulfuric acid (H_2SO_4), and methanol (CH_3OH) were purchased from Sigma–Aldrich and used as received. Deionized water was used throughout.

2.2. Synthesis of CNFs

A DMF solution of 8 wt% PAN was prepared at 60 °C, with mechanical stirring for 3 h. The electrospinning was conducted using a Gamma ES40P-20W/DAM variable high voltage power supply under a voltage of 15 kV. Under high voltage, a polymer jet was ejected through a syringe and accelerated toward the nanofiber collector, during which the solvent was rapidly evaporated. Aluminum foil was placed over the collector plate of the electrospinning apparatus to collect electrospun PAN fibers. These PAN nanofibers were first stabilized in an air atmosphere at 280 °C for 2 h at the heating rate 5 min^{-1} and then carbonized at 700 °C for 1 h in nitrogen atmosphere at the heating rate 2 °C min^{-1}. The resultant CNFs formed free-standing nonwoven membranes and were directly used as a support in the chemical deposition of PtRu nanoparticles.

2.3. 1-AP functionalization of CNFs

CNFs (0.2 g) and 1-AP (0.2 g) were added into an ethanol solution (30 ml), which was stirred mechanically for 1 h and stored at room temperature for 24 h. The solution was then filtered and washed with water for several times, and the treated CNFs were dried in a vacuum oven at 70 °C for 5 h and collected as 1-aminopyrene functionalized CNFs (1-AP-CNFs). For comparison, CNFs were also functionalized by a conventional acid treatment, *i.e.*, CNFs (0.2 g) were refluxed in a mixed strong acid solution (50 ml H_2SO_4:HNO_3 in 3:1 (v/v) ratio) at 80 °C for 3 h. The acid-treated CNFs are denoted as AO-CNFs.

2.4. Synthesis of PtRu/CNF catalysts

To deposit PtRu nanoparticles on 1-AP-CNFs, 1-AP-CNFs (0.3 g) were mixed with approximate amount of $H_2PtCl_6{\cdot}xH_2O + RuCl_3$ (with metal loadings of 25, 50, and 75 wt%, atomic Pt:Ru = 3:2) in 50 ml ethylene glycol solution under ultrasonication. The solution was then refluxed in 70 °C for almost 6.0 h until the solution changed from light yellow to dark brown, indicating the reduction and formation of PtRu nanoparticles on CNFs. The above solution was filtered and washed with water several times, and the resultant PtRu/1-AP-CNFs were soaked in water for 12 h and then dried in vacuum at 100 °C for 24 h to remove un-reacted 1-AP. PtRu/acid-functionalized CNFs (PtRu/AO-CNFs) with a PtRu metal loading of 75 wt% were also prepared using the same procedure.

2.5. Structural characterization of PtRu/1-AP-CNFs

X-ray diffraction (XRD) analysis was performed with a Philips XLF ATPS XRD 100 diffractometer using CuKα radiation (λ = 1.5405 Å). The operating voltage and current were 40.0 kV and 60.0 mA, respectively. Raman spectra of PtRu/CNFs were obtained using Horiba Jobin Yvon LabRam Aramis Microscope with 633 nm HeNe Laser.

The structure of CNFs, PtRu/AO-CNFs, and PtRu/1-AP-CNFs, which were deposited onto 200 mesh carbon-coated Cu grids, was evaluated using a Hitachi HF-2000 TEM at 200 kV. The diameters of Pt nanoparticles were determined by measuring 80 randomly selected particles using ImageJ software.

2.6. Electrochemical properties of PtRu/CNFs

The electrochemical measurements of PtRu/CNFs were performed in a three-electrode cell at 25 °C on an electrochemical workstation (AQ4 Gamry Reference 600, USA). The cell consisted of a working electrode (PtRu/CNFs), a counter electrode (Pt), and a reference electrode (Ag/AgCl/4.0 M KCl). Nitrogen was bubbled through the testing solutions for at least 30 min before the measurements, and then was used continually to protect the experiment environment. All the electrochemical potentials were measured and reported with respect to Ag/AgCl/4.0 M KCl.

Cyclic voltammetric (CV) studies of PtRu/CNFs were carried out in 0.5 M H_2SO_4 at 50 mV s^{-1} to determine the electrochemically active surface area. CV responses of PtRu/CNFs in 0.125 M CH_3OH + 0.2 M H_2SO_4 at 5 mV s^{-1} were also measured to study their activities on the methanol oxidation.

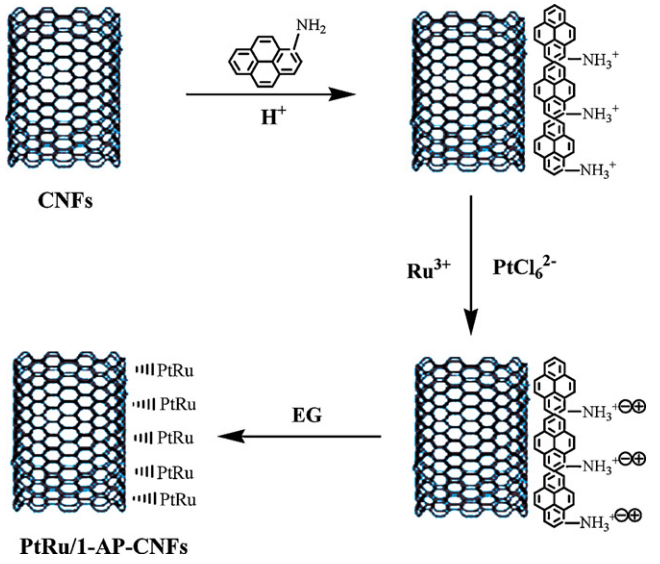

Fig. 1. Schematic diagram of the deposition of PtRu electrocatalyst on 1-AP-CNFs.

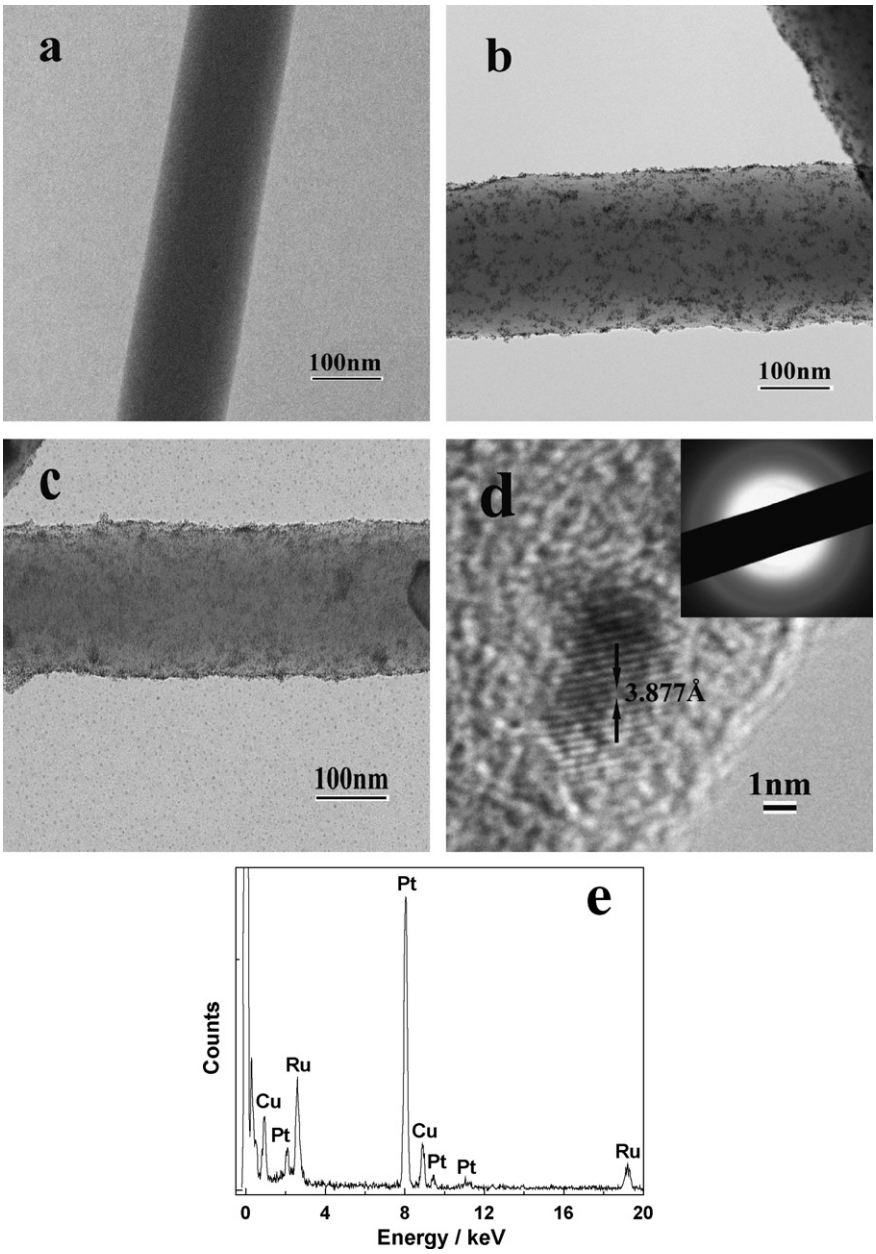

Fig. 2. TEM images of CNFs (a), PtRu/1-AP-CNFs with metal loadings of 25 wt% (b), and 50 wt% (c), high resolution TEM image and inserted electron diffraction pattern (d), and EDS spectrum (e) of PtRu/1-AP-CNFs (metal loading: 25 wt%).

3. Results and discussions

3.1. CNF treatment and PtRu deposition

Fig. 1 shows the schematic diagram of the synthesis procedure of PtRu/1-AP-CNFs. Since the surface of CNFs is chemically inert and does not have any functional groups, PtRu deposition on untreated CNF surface is not well controlled. In order to surface treat CNFs, a noncovalent functionalization involving a reagent 1-AP was used. The reagent 1-AP, a bi-functional molecule with a pyrenyl group and an amino functional group, does not have direct chemical reaction with CNFs. Typically, the pyrenyl group of 1-AP can be attached onto the basal plane of graphite via π-stacking [25]. As a result, 1-AP can be immobilized on CNFs through the adsorption of pyrenyl groups onto the inherently hydrophobic surface of CNFs. After the immobilization of 1-AP, $H_2PtCl_6{\cdot}xH_2O$ and $RuCl_3$ were added and the pH value of the solution is controlled to around 6.0 (*i.e.*, slightly acid). After that, the amino groups of immobilized 1-AP molecules become positively charged, which may lead to the self-assembly of negatively charged Pt precursors, $PtCl_6^{2-}$ ions, followed by the subsequent self-assembly of positively charged Ru precursors, Ru^{3+}. As a result, the uniform distribution of Pt and Ru precursors can be obtained on the surface of CNFs. After that, in the presence of ethylene glycol, self-assembled PtRu precursors are reduced to form PtRu nanoparticles on the CNF surface. Therefore, during the synthesis of 1-AP-CNFs, the $PtCl_6^{2-}$ and Ru^{3+} ions are attached onto CNF surface first, and then are reduced to PtRu nanoparticles.

3.2. TEM images of PtRu/1-AP-CNFs

Fig. 2 shows TEM images of CNFs and PtRu/1-AP-CNFs. In Fig. 2a, CNFs exhibit long and straight fibrous morphology with relatively uniform diameters between 100 and 300 nm. Before deposition, the CNF surface is smooth and there are no particles loaded. How-

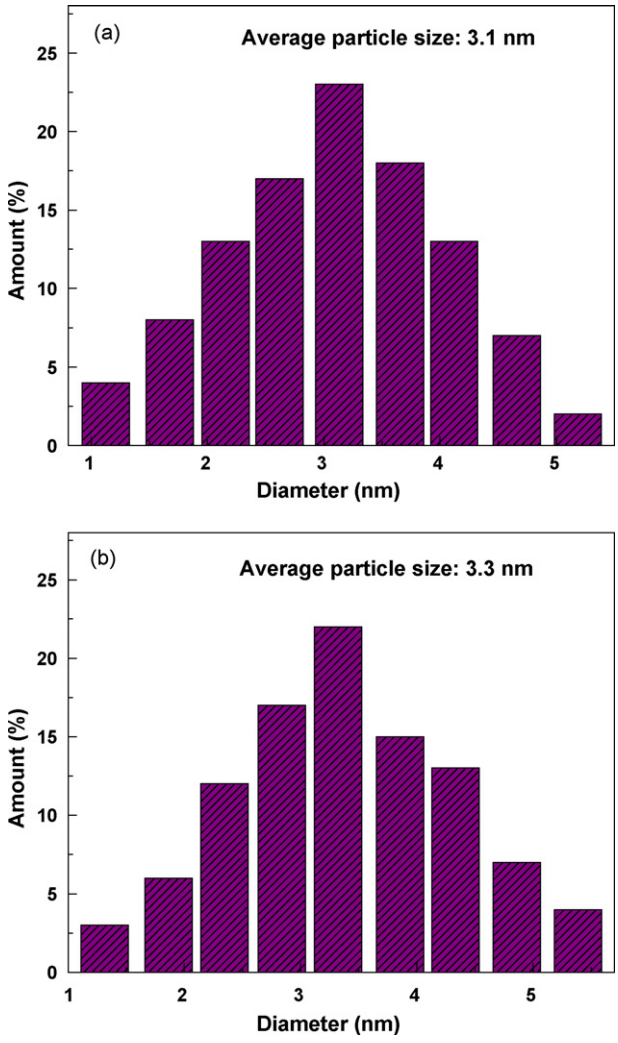

Fig. 3. Diameter distributions of PtRu nanoparticles on PtRu/1-AP-CNFs with the metal loadings of 25 wt% (a), and 50 wt% (b).

ever, PtRu nanoparticles are observed on the surface of CNFs after deposition (Fig. 2b and c). When the metal loading is 25 wt%, PtRu nanoparticles are evenly distributed on the surface of 1-AP-CNFs (Fig. 2b) and the average diameter of PtRu nanoparticles is about 3.1 nm (Fig. 3a). When the metal loading increases (*i.e.*, 50 wt%), more PtRu nanoparticles are found on the surface of 1-AP-CNFs and they are still evenly distributed. Although there is a relatively large increase in the metal loading, the average diameter of PtRu nanoparticles increases from 3.1 to 3.3 nm (Fig. 3b), which is attributed to the surface treatment of CNFs by 1-AP functionalization. A more detailed explanation is provided in Section 3.3.

Fig. 2d and e shows the high resolution TEM image, inserted electron diffraction pattern, and energy dispersive X-ray spectroscopy (EDS) of PtRu/1-AP-CNFs (metal loading: 25 wt%), respectively. In Fig. 2d, the pattern for a crystal structure of PtRu nanoparticle with crystal lattice of 3.877 Å is shown. The EDS data in Fig. 2e also confirm the presence of PtRu particles on the surface of 1-AP-CNFs, and the copper peaks belong to the TEM grid background.

3.3. Structure comparison of PtRu/1-AP-CNFs and PtRu/AO-CNFs

Fig. 4 shows TEM images and diameter distributions of PtRu/1-AP-CNFs and PtRu/AO-CNFs. The metal loading amount is the same (*i.e.*, 75 wt%) for both PtRu/CNFs. As shown in Fig. 4a, the surface of 1-AP-CNFs is almost fully covered by PtRu nanoparticles,

Table 1
Quantitative data of Pt–Ru alloy particles on PtRu/CNFs from XRD and XPS analysis. The metal loading is 75 wt%.

PtRu/CNFs	Pt/Ru ratios obtained by XRD (at.%)	Pt/Ru ratios obtained by XPS (at.%)	Nominal Pt/Ru ratios (at.%)
PtRu/AO-CNFs	68/32 ± 5	54/46 ± 2	60/40
PtRu/1-AP-CNFs	64/36 ± 5	52/48 ± 2	60/40

however, no large aggregates of PtRu particles are found. Moreover, at 75 wt% metal loading, more PtRu nanoparticles are evenly distributed on the surface of 1-AP-CNFs and the particle size of PtRu electrocatalysts on 1-AP-CNFs increases slightly to 3.6 nm, as compared to those with metal loadings of 25 and 50 wt%. For AO-CNFs, which were oxidized in a mixed strong acid solution (50 ml H_2SO_4:HNO_3 in 3:1 (v/v) ratio) at 80 °C, PtRu nanoparticles can also be found on the fiber surface. However, the average size of PtRu nanoparticles increases to 5.4 nm, and the particles are aggregated significantly. The relatively small size of PtRu nanoparticles on PtRu/1-AP-CNFs could be caused by the immobilization of bi-functional 1-AP molecules, which offer large and uniformly distributed active sites for anchoring $PtCl_6^{2-}$ and Ru^{3+} ions and subsequently Pt and Ru nanoparticles (Fig. 1). Thus, compared with conventional acid-oxidized CNFs, 1-AP-functionalized CNFs are more effective for use as catalyst supporting materials.

3.4. XRD patterns of PtRu/1-AP-CNFs and PtRu/AO-CNFs

X-ray diffraction (XRD) profiles of PtRu/1-AP-CNFs and PtRu/AO-CNFs are presented in Fig. 5. For comparison, the XRD profile of untreated CNFs is also shown. The diffraction peak at around 25° can be assigned to the diffraction of the (0 0 2) plane of graphite layers in CNFs. The XRD profiles of PtRu/AO-CNFs and PtRu/1-AP-CNFs also confirm that the PtRu phase is formed on both CNFs and can be indexed to the reflections of crystal structure of PtRu nanoparticles at 39.9° (1 1 1), 45.8° (2 0 0), 68.3° (2 2 0), and 82.0° (2 2 2), respectively. The diffraction peaks of PtRu/1-AP-CNFs are stronger than those of PtRu/AO-CNFs due to their smaller PtRu particle size that makes the XRD measurement more sensitive.

Moreover, the Pt–Ru alloy compositions of PtRu/CNFs were calculated from the simple mathematical expression of Vegard's law [26,27]:

$$a_{PtRu} = (1 - x)a_{Pt} + xa_{Ru} \quad (2)$$

where a_{PtRu}, a_{Pt}, and a_{Ru} are the lattice parameters of Pt–Ru alloy, pure Pt, and pure Ru, respectively, and x the mole fraction of the component Ru. The lattice parameters of pure Pt and pure Ru are 3.92 and 3.79 Å [28], respectively. When the composition of Ru is lower than 60 at.%, Pt and Ru form a face-centered cubic (fcc) structure. Based on the XRD profiles in Fig. 5, a value of 3.879 ± 0.005 Å for the lattice parameter of Pt–Ru alloy on PtRu/AO-CNFs and a value of 3.873 ± 0.005 Å for Pt–Ru alloy on PtRu/1-AP-CNFs were determined by the peak profile fitting of the (2 2 0) reflection shown in Fig. 5, which correspond to 32 ± 5 and 36 ± 5 at.% of Ru in the Pt–Ru alloy (Table 1).

3.5. XPS spectrum of PtRu/1-AP-CNFs

X-ray photoelectron spectroscopy (XPS) spectrum obtained from PtRu/1-AP-CNFs is presented in Fig. 6. One characteristic peak of *4d* for Pt appears at about 315 eV, two characteristic peaks of *3p* for Ru appear at around 461 and 484 eV, and one *1s* peak of carbon appears at about 285 eV, respectively. Since the oxidation state of Ru is important for its catalytic activity, the high resolution XPS data were investigated and the results show that the oxidation state

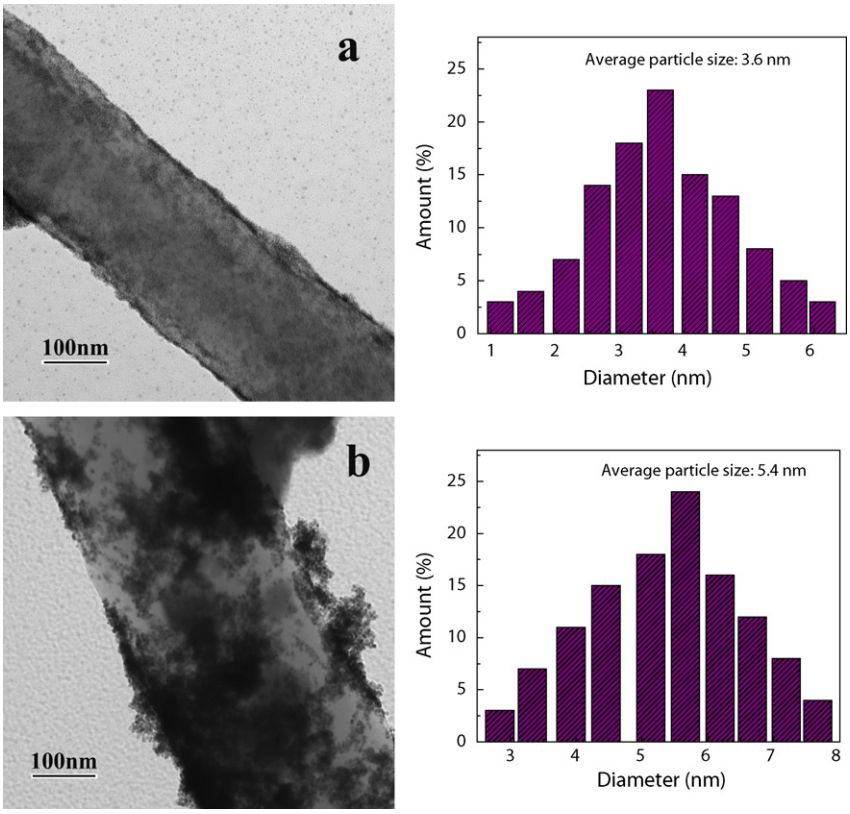

Fig. 4. TEM images and PtRu diameter distributions of PtRu/1-AP-CNFs (a), and PtRu/AO-CNFs (b). The metal loading is 75 wt%.

of Ru is zero-valent, which confirms the formation of Pt–Ru alloy. Moreover, based on the intensities of XPS peaks of Pt *4d* and Ru *3p*, the atomic ratios of Pt/Ru on PtRu/1-AP-CNFs and PtRu/AO-CNFs were calculated to be 52.3/47.7 and 55.4/45.6, respectively, which are comparable to the molar ratio of Pt and Ru precursors used in the preparation of PtRu/1-AP-CNFs and PtRu/AO-CNFs (Table 1).

3.6. Raman spectra of PtRu/1-AP-CNFs and PtRu/AO-CNFs

Raman spectra of untreated CNFs, PtRu/1-AP-CNFs, and PtRu/AO-CNFs are shown in Fig. 7. Raman spectra of carbon materials reflect the electronic structure and electron-phonon interactions and allow clear identification of graphite layers [29]. The peak at 1335 cm^{-1} is assigned to the disordered graphite structure (*D*-band), and the frequency peak at 1587 cm^{-1} (*G*-band) corresponds to a splitting of the E_{2g} stretching mode of graphite, which reflects the structural intensity of the sp^2-hybridized carbon atoms [30]. Therefore, the intensity ratio of *D*- and *G*-bands (I_D/I_G) can be used to evaluate the extent of the modification or defects on CNF surface and a higher I_D/I_G ratio typically indicates a higher degree of disorder. From Fig. 7, the I_D/I_G ratio of PtRu/AO-CNFs increases from 1.30 to 1.49 as compared to untreated CNFs. This indicates that the harsh acid treatment produces carboxylic acid sites on the surface, causing significant structural damage on

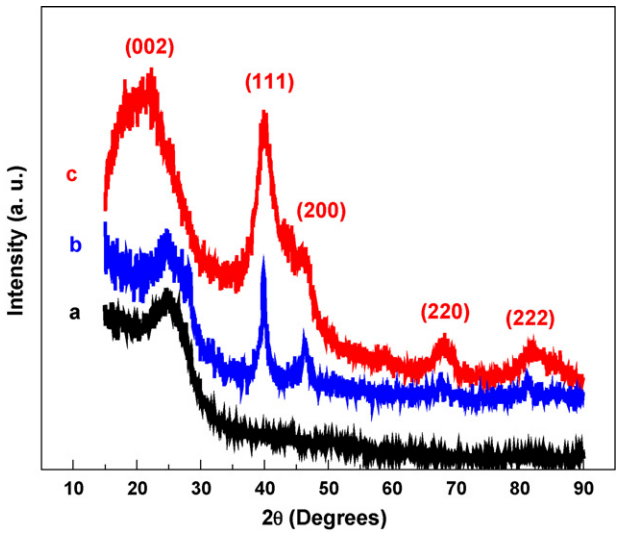

Fig. 5. XRD profiles of CNFs (a), PtRu/AO-CNFs (b), and PtRu/1-AP-CNFs (c). The metal loading is 75 wt%.

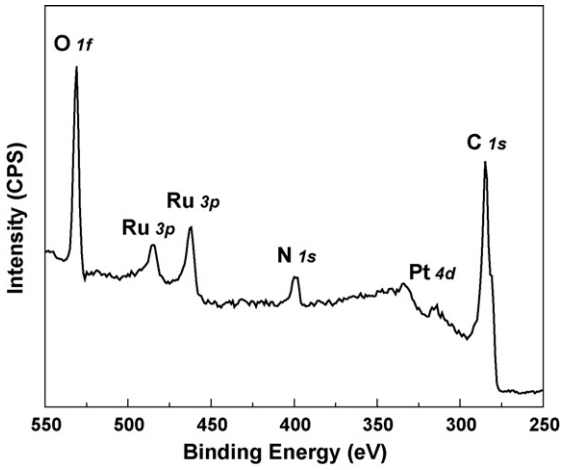

Fig. 6. XPS spectrum of PtRu/1-AP-CNFs in the binding energy range of 550-250 eV. The metal loading is 75 wt%.

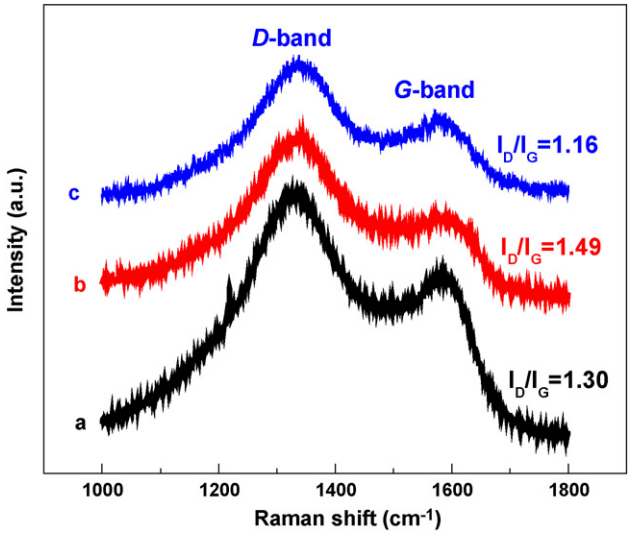

Fig. 7. Raman spectra of CNFs (a), PtRu/AO-CNFs (b), and PtRu/1-AP-CNFs (c). The metal loading is 75 wt%.

the ordered structure of CNF surface. PtRu/1-AP-CNFs have slightly lower I_D/I_G ratio (*i.e.*, 1.16, Fig. 7) than untreated CNFs, which indicates that the immobilization or wrapping of 1-AP on the surface of CNFs via π-stacking has no detrimental effect on the ordered structure in CNFs. Rather, the slightly decreased ratio may suggest the coverage of the original defect sites by 1-AP molecules.

3.7. Electrochemical characterization of PtRu/1-AP-CNFs and PtRu/AO-CNFs

CV measurements of PtRu/AO-CNFs and PtRu/1-AP-CNFs between −0.2 and +1.0 V at 50 mV s^{-1} in 0.5 M H_2SO_4 were employed to examine whether PtRu particles on CNF surface are electrochemically active (Fig. 8). The redox current density peaks can be observed, which are due to the adsorption and desorption of hydrogen at the surface of PtRu nanoparticles on CNFs.

The integration of CV curves from hydrogen desorption peaks from −0.2 to +0.2 V gives electrochemical active surface area (EASA), which can be calculated according to the following formula

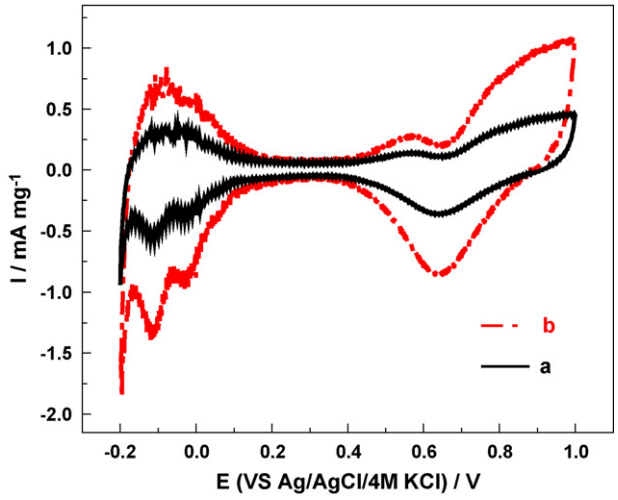

Fig. 8. Current–potential curves of PtRu/AO-CNFs (a), and PtRu/1-AP-CNFs (b) in 0.5 M H_2SO_4 at 50 mV s^{-1}. The metal loading is 75 wt%.

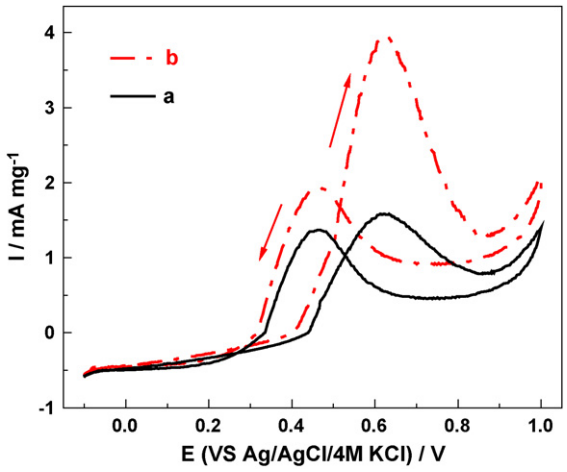

Fig. 9. Stabilized current–potential curves of PtRu/AO-CNFs (a), and PtRu/1-AP-CNFs (b), in 0.125 M CH_3OH + 0.2 M H_2SO_4 at 5 mV s^{-1}. The metal loading is 75 wt%.

[31]:

$$\text{EASA} = \frac{Q(\text{mC mg}^{-1})}{0.22(\text{mC cm}^{-2})} \quad (3)$$

where Q is the electric charge for hydrogen desorption and 0.22 mC cm^{-2} is the hydrogen adsorption constant (based on Pt). Table 2 shows the calculated EASA values for both PtRu/AO-CNFs and PtRu/1-AP-CNFs. The EASA for PtRu/1-AP-CNFs is 327 ± 5 cm^2 mg^{-1}, much higher than that of PtRu/AO-CNFs (233 ± 5 cm^2 mg^{-1}), which is due to the smaller PtRu particle size and less agglomerate formation on the surface of 1-AP-CNFs. Therefore, the PtRu nanoparticles deposited on 1-AP-CNFs are electrochemically more accessible, which is important for electrocatalyst applications in fuel cells.

3.8. Electro-oxidation of methanol on PtRu/CNFs

Fig. 9 shows the stabilized current density-potential curves of PtRu/AO-CNFs and PtRu/1-AP-CNFs in 0.125 M CH_3OH + 0.2 M H_2SO_4 (pH 0.45 ± 0.05) solution at 5 mV s^{-1}. Both PtRu/AO-CNFs and PtRu/1-AP-CNFs present the electro-oxidation of methanol, which starts at around +0.40 V and then the current density increases to a maximum at about +0.63 V; moreover, another current peak is found at about +0.43 V when scanning back. The mechanism for the methanol reaction is: first, methanol is adsorbed on the freshly reduced PtRu nanoparticles surface produced after the removal of non-reacting PtRu–O species, and then transformed to different reactive intermediates, such as $(CH_2O)_{ads}$ and $(CHO)_{ads}$, and poisoning species $(CO)_{ads}$. Both reactive and poisoning species can be further oxidized to CO_2, however, a relatively higher potential is required to oxidize the poisoning species $(CO)_{ads}$ [32–35].

In order to study the efficiency of methanol oxidation, the electrochemical characteristic data of PtRu/AO-CNFs and PtRu/1-AP-CNFs are summarized in Table 2. The efficiencies of methanol oxidation were compared in terms of forward onset potential, CO-tolerant current density at +0.45 V, forward peak current density (I_f), and the ratio of forward to backward peak current densities (I_f/I_b) [36,37]. From Table 2, compared with PtRu/AO-CNFs, PtRu/1-AP-CNFs have larger CO-tolerant current density and forward peak current density due to their reduced PtRu particle size and increased EASA. The I_f/I_b ratio of PtRu/1-AP-CNFs is also larger than that of PtRu/AO-CNFs, which may be related to the smaller PtRu particles in PtRu/1-AP-CNFs. In addition, a smaller forward onset potential is obtained at PtRu/1-AP-CNFs, indicating the better catalytic activity of PtRu/1-AP-CNFs than that of PtRu/AO-CNFs.

Table 2
Electrochemical characteristics of PtRu/AO-CNFs and PtRu/1-AP-CNFs. Solutions: 0.5 M H_2SO_4 for EASA and 0.125 M CH_3OH + 0.2 M H_2SO_4 (pH 0.45 ± 0.05) for other characteristics. Scanning rate: 5 mV s^{-1}. The metal loading is 75 wt%.

Catalysts	Average particle size (nm)	EASA ($cm^2\ mg^{-1}$)	Onset potential (V vs. Ag/AgCl/4.0 M KCl)	CO-tolerant current density at +0.45 V ($mA\ mg^{-1}$)	Forward peak current density (I_f, $mA\ mg^{-1}$)	I_f/I_b
PtRu/AO-CNFs	5.4 ± 0.3	233 ± 5	0.42 ± 0.02	0.13 ± 0.01	1.58 ± 0.02	1.08 ± 0.01
PtRu/1-AP-CNFs	3.6 ± 0.3	327 ± 5	0.39 ± 0.02	0.52 ± 0.01	3.93 ± 0.02	2.07 ± 0.01

4. Conclusions

The preparation and characterization of PtRu/CNFs by the combination of 1-AP functionalization and a polyol processing technique were studied. PtRu nanoparticles with well-defined morphology and good catalyst activity were obtained on functionalized CNFs. Compared with the conventional acid-treated CNFs, the simple synthesis process of 1-AP-functionalization treatment can preserve the integrity and the electronic structure of CNFs. The diameter of PtRu nanoparticles on 1-AP functionalized CNFs is around 3.5 nm, which is smaller than that of PtRu/CNFs prepared from the conventional acid-treated CNFs. Moreover, PtRu nanoparticles are much more evenly distributed on 1-AP functionalized CNFs and do not form agglomerates. The resulting PtRu/1-AP-CNFs possess the properties of higher active surface area and better performance towards the oxidation of methanol. Therefore, the chemical deposition of PtRu nanoparticles on 1-AP-CNFs provides an alternative method to obtain an effective catalyst toward the oxidation of methanol. However, investigations into the catalytic ability of such composites in membrane electrode assembly in direct methanol fuel cells are needed for future applications.

Acknowledgements

This work was supported by the National Textile Center (ITA-08-07400), U.S. National Science Foundation (0833837), and ACS Petroleum Research Fund (47863-G10).

References

[1] K.Y. Chan, J. Ding, J.W. Ren, S.A. Cheng, K.Y. Tsang, J. Mater. Chem. 14 (2004) 505.
[2] V. Mehta, J.S. Cooper, J. Power Sources 114 (2003) 32.
[3] C. Yang, S. Srinivasan, A.S. Arico, P. Creti, V. Baglio, V. Antonucci, Electrochem. Solid-State Lett. 4 (2001) A31.
[4] N. Wakabayashi, H. Uchida, M. Watanabe, Electrochem. Solid-State Lett. 5 (2002) E62.
[5] P.S. Kauranen, E. Skou, J. Munk, J. Electroanal. Chem. 404 (1996) 1.
[6] M. Watanabe, S. Motoo, J. Electroanal. Chem. 60 (1975) 267.
[7] K.P. De Jong, J.W. Geus, Cat. Rev.—Sci. Eng. 42 (2000) 481.
[8] J. Guo, G. Sun, Q. Wang, G. Wang, Z. Zhou, S. Tang, L. Jiang, B. Zhou, Q. Xin, Carbon 44 (2006) 152.
[9] Z.B. He, J.H. Chen, D.Y. Liu, H. Tang, W. Deng, W.F. Kuang, Mater. Chem. Phys. 85 (2004) 396.
[10] K. Lee, J. Zhang, H. Wang, D.P. Wilkinson, J. Appl. Electrochem. 36 (2006) 507.
[11] K. Shimazu, D. Weisshaar, T. Kuwana, J. Electroanal. Chem. 223 (1987) 223.
[12] Y.N. Xia, P.D. Yang, Y.G. Sun, Y.Y. Wu, B. Mayers, B. Gates, Y.D. Yin, F. Kim, Y.Q. Yan, Adv. Mater. 15 (2003) 353.
[13] B.K. Balan, S.M. Unni, S. Kurungot, J. Phys. Chem. C 113 (2009) 17572.
[14] Z.P. Guo, D.M. Han, D. Wexler, R. Zeng, H.K. Liu, Electrochim. Acta 53 (2008) 6410.
[15] A.D. Taylor, R.C. Sekol, J.M. Kizuka, S. D'Cunha, C.M. Comisar, J. Catal. 259 (2008) 5.
[16] G.L. Che, B.B. Lakshmi, E.R. Fisher, C.R. Martin, Nature 393 (1998) 346.
[17] S.H. Joo, S.J. Choi, I. Oh, J. Kwak, Z. Liu, O. Terasaki, R. Ryoo, Nature 412 (2001) 169.
[18] Z.Q. Tian, S.P. Jiang, Y.M. Liang, P.K. Shen, J. Phys. Chem. B 110 (2006) 5343.
[19] X. Wang, W.Z. Li, Z.W. Chen, M. Waje, Y.S. Yan, J. Power Sources 158 (2006) 154.
[20] L. Cao, F. Scheib, C. Roth, F. Schweiger, C. Cremers, U. Stimming, H. Fuess, L. Chen, W. Zhu, X. Qiu, Angew. Chem. Int. Ed. 45 (2006) 5315.
[21] S.Y. Wang, X. Wang, S.P. Jiang, Langmuir 24 (2008) 10505.
[22] M.A. Correa-Duarte, N. Sobal, L.M. Liz-Marzan, M. Giersig, Adv. Mater. 16 (2004) 2179.
[23] Y.Y. Ou, M.H. Huang, J. Phys. Chem. B 110 (2006) 2031.
[24] D.Q. Yang, J.F. Rochette, E. Sacher, J. Phys. Chem. B 109 (2005) 4481.
[25] H. Jaegfeldt, T. Kuwana, G. Johansson, JACS 105 (1983) 1805.
[26] A.R. Denton, N.W. Ashcroft, Phys. Rev. A 43 (1991) 3161.
[27] M.J. Lambregts, S. Frank, Talanta 62 (2004) 627.
[28] M.S. Nashner, A.I. Frenkel, D.L. Adler, J.R. Shapley, R.G. Nuzzo, J. Am. Chem. Soc. 119 (1997) 7760.
[29] A.C. Ferrari, J.C. Meyer, V. Scardaci, C. Casiraghi, M. Lazzeri, F. Mauri, S. Piscanec, D. Jiang, K.S. Novoselov, S. Roth, A.K. Geim, Phys. Rev. Lett. (2006), 97.
[30] M.S. Dresselhaus, G. Dresselhaus, R. Saito, A. Jorio, Phys. Rep. 409 (2005) 47.
[31] S.L. Knupp, W.Z. Li, O. Paschos, T.M. Murray, J. Snyder, P. Haldar, Carbon 46 (2008) 1276.
[32] D. Pletcher, J. Appl. Electrochem. 14 (1984) 403.
[33] P.N. Ross, Electrochim. Acta 36 (1991) 2053.
[34] A. Kabbabi, R. Faure, R. Durand, B. Beden, F. Hahn, J.M. Leger, C. Lamy, J. Electroanal. Chem. 444 (1998) 41.
[35] F. Kadirgan, B. Beden, J.M. Leger, C. Lamy, J. Electroanal. Chem. 125 (1981) 89.
[36] H. Laborde, J.M. Leger, C. Lamy, J. Appl. Electrochem. 24 (1994) 219.
[37] M.C. Tsai, T.K. Yeh, C.H. Tsai, Electrochem. Commun. 8 (2006) 1445.